SIMULATION OF THE RESONANT INTERACTIONS BETWEEN A BOUNDARY LAYER AND AN ARRAY OF DEEP CAVITIES

Grigory Shelekhov[1*], **Julien Bodart**[1] **and Laurent Joly**[1]
1: DAEP, ISAE-SUPAERO
10 av. Edouard Belin, Toulouse
*Correspondent author: grigory.shelekhov@isae.fr

ABSTRACT

We have performed numerical simulations of the interaction between a laminar boundary layer flow and an array of deep slit-aperture cavities solving fully compressible Navier-Stockes equations with a finite-volume solver `CharLES`^{X}. The cavities are included in the computational domain which allows to study the full interaction *i.e.* the excitation mechanism of the liner and its acoustic response. The parameter space is explored by varying the cavity depth D, thus shifting the cavity resonant modes $f_{r,m} = (2m-1)\frac{c}{4D}$, where m is a positive integer. Four cases, with varying cavity depth were studied. In all cases, the coupling of the grazing shear layer instabilities to the acoustic standing waves inside cavities (resonant interaction) leads to the generation of large Kelvin-Helmholtz (KH) rollers, scaling as $\lambda_{KH} = U_c/f_{r,1}$. In some cases, this coupling leads to the excitation of $m > 1$ resonant modes in the upstream cavities. However vortex merge occurring over the cavities switches the mode $m = 1$ further downstream. Overall, the results suggest that an array of deep cavities has a promising potential application for passive flow control.

1 Introduction

Acoustic liners are devices commonly used to attenuate noise emissions for engineering applications. However, multiple studies have shown that development of that hydrodynamic instabilities may be triggered over low-resistance liners. Pursuing the experimental investigations of Meyer *et al.* (1958), Brandes & Ronneberger (1995) and Jüschke (2006) studied a model liner consisting of an array of thin-walled deep slit-aperture cavities under acoustic excitation, in a duct flow configuration. In their measurements, the sound transmission coefficient is greater than one for frequencies f around the liner resonance frequency f_r, suggesting sound generation. Specifically, the sound generation is maximal for f slightly above the liner resonance frequency. Such behavior was attributed to the presence of an instability over the liner. Flow visualization performed in the vicinity of the liner demonstrating the instability was carried out using PIV and LDV measurements by Marx *et al.* (2010) in a duct flow interacting with a liner characterized with a similar geometry as in Jüschke (2006). The authors measured the instability wavelength, amplification rate and its phase velocity. Phase-averaged visualization evidences the presence of the spanwise coherent periodic flow structures over the liner surface. Theoretical stability studies (Rienstra & Darau, 2011; Scalo & Rahbari, 2015; Marx & Aurégan, 2010) have been able to predict unstable modes and inform on the threshold parameters to trigger the instability. A major difficulty for stability analysis lies in the choice of a relevant base flow, as the flow undergoes a rapid evolution over the liner (*e.g.* experimental results by Marx *et al.* (2010)). In these studies, the orifice-by-orifice response of the liner is classically modeled through an homogeneous Impedance Boundary Condition (IBC):

$$\hat{p} = \rho_0 c_0 Z(\omega)\hat{v} \tag{1}$$

where $Z(\omega)$ is the dimensionless specific acoustic impedance, a complex function of the angular frequency, characterized by a real part (resistance) $Re(Z) = R$, and an imaginary part (reactance) $Im(Z) = \chi$. $\hat{p}$ denotes the acoustic pressure, while $\hat{v}$ is the wall-normal acoustic velocity. ρ_0 and c_0 are respectively the base density and the base sound speed. Similarly, most numerical simulations solving Navier-Stokes equations rely on liner modeling by imposing (1) either in spectral domain or in time domain, which allows for reducing the computational cost. Xin *et al.* (2016) computed the sound transmission coefficients and the velocity fluctuations in a partially lined duct using Linearized Navier-Stokes Equations (LNSE) with eddy viscosity formulated in frequency domain, using the same geometry as in Marx *et al.* (2010). By taking into account the spatial evolution of the flow field using experimental data from Marx *et al.* (2010), authors obtained a good agreement of the computed transmission coefficient when compared with experimental results. However the fluctuation wall-normal velocity amplitudes in the vicinity of the liner remain significantly under-predicted. Burak *et al.* (2009) used LNSE simulations to study the instability over the liner. The base flow required for the LNSE computations was provided using compressible RANS simulations, and an instability pattern was detected in cases with appropriate resolution at the boundary.

In contrast to frequency-domain solvers, exact imposition of (1) in the time domain and its coupling to an unsteady Navier-Stokes solver calls for using particular computational methods. Burak *et al.* (2009) coupled a Navier-Stokes solver with slip wall conditionad and the Time-Domain Impedance Boundary Condition (TD-IBC) of Tam & Auriault (1996). Large eddy simulations of fully developed turbulent channel flow (Scalo *et al.*, 2015) provided evidence that, low-resistance IBC ($R = 0.01, R = 0.1$) triggers hydrodynamic instability without explicit acoustic forcing. The observed increased of wall-normal veloc-

ity fluctuations v_{rms} in the near-wall region is consistent with the experimental measurements of Marx *et al.* (2010), which shows up to 28% increase of v_{rms} on the lined side of the duct, without acoustic excitation. While existing studies clearly demonstrate that an hydrodynamic instability may develop over the liner, the physical mechanisms of this phenomenon remain unclear. To further understand these phenomena, one may incorporate the cavities within the computational domain, which allows to obtain time-resolved data in the orifice region. Although these data could be obtained using experiments, the small size of the cavities prevents detailed characterization of the flow field in the cavities. Recently, Zhang & Bodony (2016) carried out simulations of the temporal development of the interaction between a single Helmholtz resonator orifice and a turbulent boundary layer at $M = 0.5$ subject to strong acoustic excitations. Due to the heavy grid requirements, the authors had to limit the study to a single cavity. In this paper we aim at performing numerical experiments to capture the relevant physical mechanisms of the boundary layer/liner interaction. The chosen liner model is a 2D geometry, which incorporates a large number of cavities and allow for the spatial development of large wavelength perturbations.

2 Problem Formulation

Experimental investigations of Marx *et al.* (2010); Brandes & Ronneberger (1995); Jüschke (2006) focused on an acoustically excited low-resistance liner, composed of an array of thin-walled deep cavity slots. In order to isolate the instability mechanisms, we consider a spatially developing two-dimensional flow over a flat plate backed by n_c deep slit-aperture cavities without acoustic forcing. Additionally, we exclude the broadband turbulence excitation by considering a laminar incoming flow. Figure 1 summarizes the main geometry parameters of the studied configuration. A possible set of dimensionless parameters governing the problem are: i) the Reynolds number based on the incoming boundary layer momentum thickness and free-stream velocity $Re_\theta = \frac{\theta U_\infty}{\nu}$, ii) the Mach number $M = \frac{U_\infty}{c}$ where c is the free-stream speed of sound, iii) the ratio of momentum thickness to the cavity aperture θ/d_x, iv) the ratio of the cavity aperture to the cavity depth d_x/D, v) the percentage of open area (or porosity) $\sigma = N_{cavities} d_x / L_{liner}$. The choice of the geometry and flow parameters is inspired by the experiment Marx *et al.* (2010). Correspondingly, the Mach number is set to $M = 0.3$ and $\theta/d = 0.6$. To further simplify the geometry, we study the limiting case in which the inter-cavity walls have a zero thickness. In comparison with the work of Marx *et al.* (2010), the porosity σ is increased from 80% to 100% due to inter-cavity zero-thickness wall assumption, while the Reynolds number is lowered from $Re_\theta = 4600$ to $Re_\theta = 2000$ (with a laminar assumption) to limit the computational cost.

As we will show further, the instability arises due to the coupling of the acoustic standing wave in the cavity and the inherent shear layer instabilities. Since $d_x \ll D$, we expect y-directed modes of the cavity to be excited. Those mode frequencies are given by (*e.g.* Hirschberg & Rienstra (2004)):

$$St_{r,m} = \frac{f_{r,m} D}{U} = \frac{(2m-1)c}{4D}, \quad m = 1, 2, 3, \ldots \qquad (2)$$

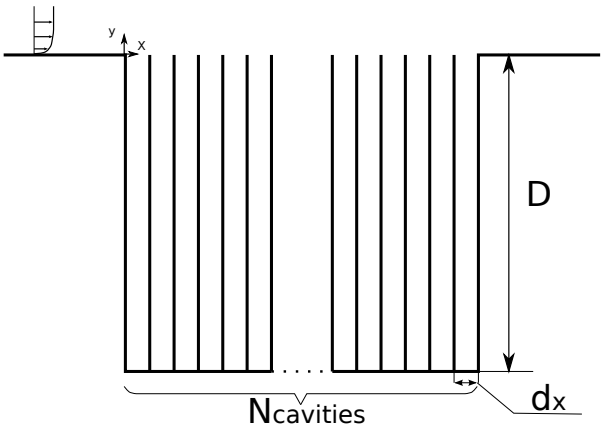

Case	N_c	d_x/θ_{in}	D/d_x	σ
A1	77	1.6	80	1.0
A2	77	1.6	40	1.0
A3	77	1.6	26	1.0
A4	77	1.6	20	1.0

Figure 1: Sketch of the geometry and summary of the parameters used for the four simulations.

3 Numerical Methodology

The numerical simulations are run using a massively parallel finite-volume solver for the fully compressible Navier-Stokes equations on unstructured grids `CharLES`^{X}. It has already been applied to a large variety of problems, ranging from shock-turbulence boundary layer interaction to high-Reynolds number flows (Moreno *et al.*, 2014; Bodart *et al.*, 2017).

Adiabatic, no-slip boundary conditions are imposed both on the flat plate and the cavities wall. The array of cavities is located $10d_x$ downstream the inflow boundary. The first cavity sets the reference $x = 0$. The grid spacing in the streamwise direction is constant for $0 \leq x \leq 144d_x$. Grid stretching is applied from $x \geq 144d_x$ to the outlet boundary at $x = 309d_x$ to ensure negligible influence in the interaction region.

The computation is initialized with a constant pressure, temperature and density equal to the inlet parameters. The instantaneous velocity profile outside the cavities is set to an empirical turbulent boundary layer *mean* profile $U/U_\infty = (y/\delta)^{1/7}$, also imposed at the inlet, while the flow is initially set at rest within the cavities. After a transient period $T_{transient} \approx 30/f_{c,0}$ (leading cavity acoustic cycles), statistics are sampled during a minimum period of $T_{sampling} = 30U_\infty/(d_x N_{cavities})$ convective time units over the entire lined region.

4 Results

The transient is essentially characterized by the amplification of the pressure fluctuation in the cavities, which eventually saturates. In all considered cases, the interaction of the flow with the cavities resulted in the generation of the coherent spanwise vortices convected in the streamwise direction, and coupled to acoustic standing waves in the cavities. Two distinct flow regions are found in all simulations: the region starting at the upstream edge of the treated zone where the instability is convectively amplified and reaches a saturated state, followed by a second region which is domi-

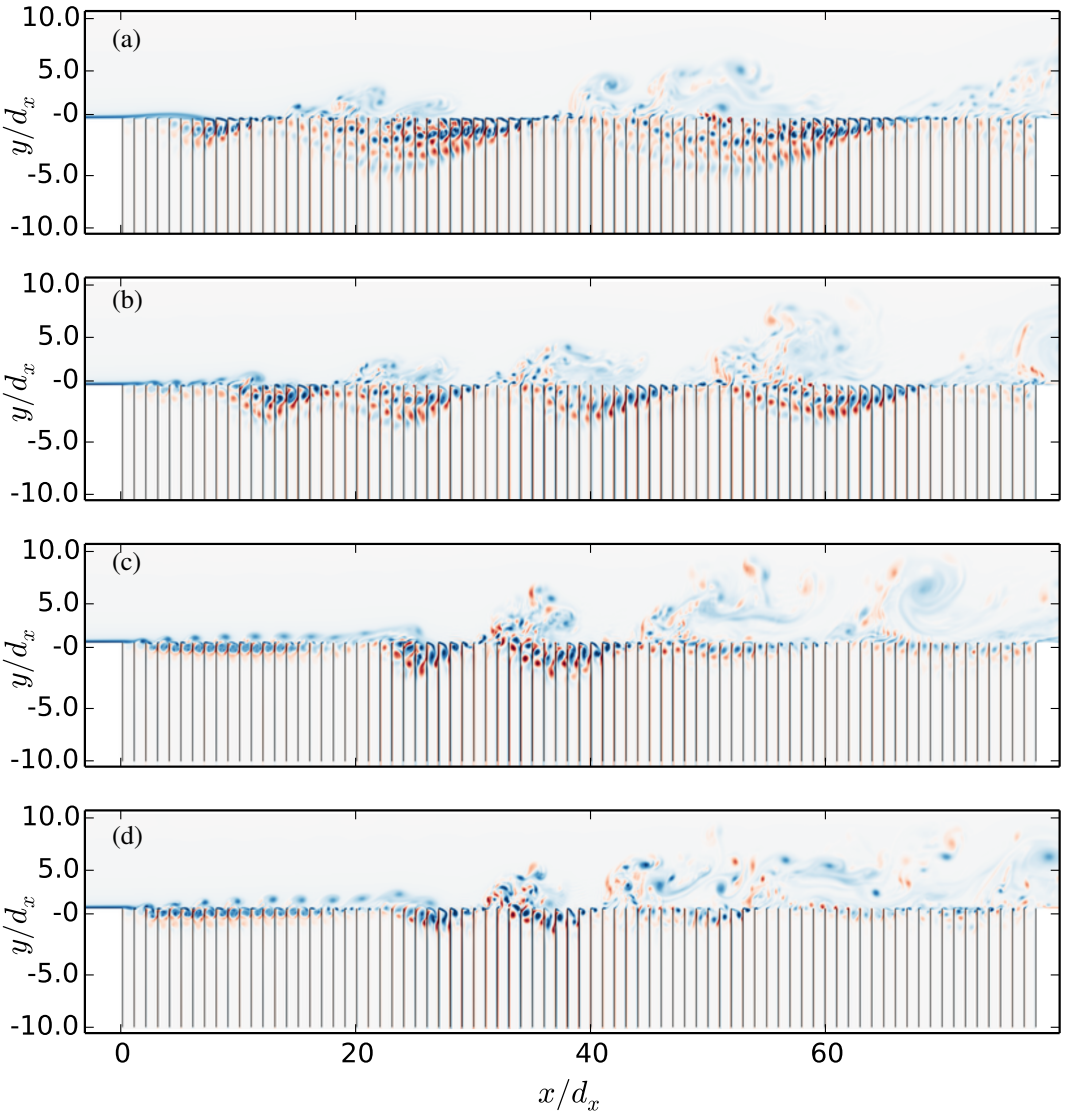

Figure 2: Visualization of the instantaneous spanwise vorticity field Ω_z for the cases (a) A1; (b) A2; (c) A3; (d) A4. Note that the cavity depth is shown partially. The spanwise vorticity ranges $-3U_\infty/d_x < \Omega_z < 3U_\infty/d_x$ (blue to red)

nated by large-scale Kelvin-Helmholtz (KH) vortices.

To characterize this vortices generation, we consider the first cavity of the liner. As shown by Elder *et al.* (1982) the mechanism of the flow-excited oscillations inside a single cavity may be understood in terms of a feedback loop including the shear layer and cavity responses. The boundary layer translates to a separated shear layer after the first cavity upstream edge. The shear layer is known to act as a disturbances amplifier, leading to the developed KH instability. Initial perturbation, which arises from numerical noise, causes periodic upward and downward flapping motion and eventually the roll-up of the shear layer. Both phenomena are characterized by unsteady vortical motion, thus associated with acoustic excitation. The cavity provides a selective response according to its multiple resonance frequencies given by (6) in the direction normal to the shear layer, further disturbing the shear layer and closing the feedback loop. In contrast to the isolated cavity case, this disturbance is convected to the next cavities ($n = 2, .., N_{cavities}$). The feedback loop described above needs to be considered for the n cavities. Each cavity provide a response to the shear layer modulated by the upstream cavity $n-1$, and further convected to the cavity $n+1$. The variation of the response over the cavities leads to the spatial modification of the shear layer characteristics over the *entire liner* downstream. In particular, it results in the imposition of specific cavity resonant modes. Figure 3 informs on the modification of the excited modes in the cavities for different streamwise positions over the liner. The PSD of the pressure fluctuations $p\prime$ is computed based on the time history of the pressure fluctuations recorded within the statistically steady state. The excitation in the first cavity is centered about the resonant modes given by the equation (6). In particular, the cases A2, A3, A4 exhibit resonances at $m > 1$ modes, specifically $m = 11$, $m = 7$, $m = 5$, centered around a Strouhal number $St = 0.24$ $St = 0.21$, $St = 0.20$, respectively. This occurrence may be explained using analytical model of the feedback loop by Elder *et al.* (1982), which, based on lin-

ear theory of Michalke (1965) provides the Strouhal number the shear layer flapping motion frequency $St = M\frac{U_c}{U} \approx 0.46$. This value requires a correction when the cavity aperture is small, *i.e.* $\delta > d_x$, to account for convection velocity variation in the proximity of the cavity no-slip walls. Applying this correction leads to a closer estimates $St = 0.14$ with the simulations. In the A1 case, resonance of this "shear layer" induced mode is not observed.

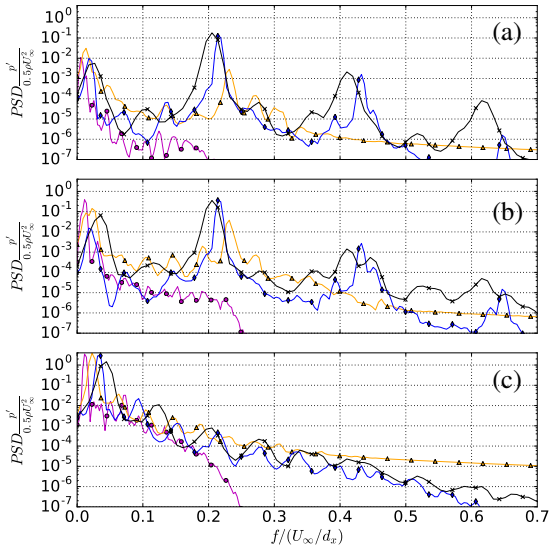

Figure 3: PSD of the pressure fluctuations measured at the bottom wall of the cavities (a) $n = 1$, (b) $n = 6$, (c) $n = 50$. (magenta) A1, (orange) A2, (blue) A3, (black) A4.

Figure 4 quantifies the evolution of the square root of the momentum coefficient $\sqrt{C_\mu}$ defined as:

$$C_\mu = \frac{2\rho_j}{\rho_\infty U_\infty^2 d_x}\int_{orifice} v_{rms}^2 dx \quad (3)$$

$$\approx \frac{2}{d_x U_\infty^2}\int_{orifice} v_{rms}^2 dx \quad (4)$$

due to weak compressibility effect and $\rho_\infty \approx \rho_j$.

denotes the per-cavity averaged intensity of response to the hydrodynamic excitation. In all cases, the spatial increase of $\sqrt{C_\mu}$ from the upstream edge of the lined zone suggests the convective amplification of the KH instability until the saturation of the linear growth mechanisms, associated with the vortex roll-up. As suggested by both the vorticity visualization and the FFT spectra, A1 the shear layer growth is coupled with the mode $m = 1$ and saturation is reached at $x \approx 20d_x$. In the cases A2, A3 and A4 the instability is initially coupled to higher resonant modes The plateau at $x = 6d_x$ and the peak at $x = 2d_x$ correspond to the spatial saturation. The cavity resonant mode is switched to $m = 1$ due to the vortex merger which increase of the rollers' wavelength as discussed in Ho & Huang (1982) and therefore the associated decrease of the cavity excitation frequency.

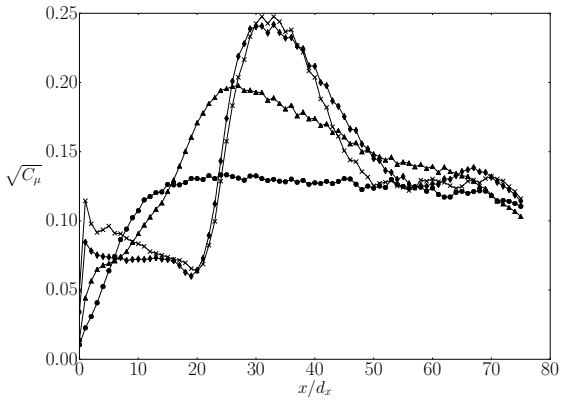

Figure 4: Square root of the momentum coefficient $\sqrt{C_\mu}$ which denotes the per-cavity averaged intensity of the induced wall-normal velocity fluctuations at the cavity-flat plate interface (filled circles): A1, (filled triangles): A2, (filled diamonds): A3, (crosses): A4

In order to further characterize the instability, the KH rollers size was measured *a-posteriori* at the downstream part of the liner and compared to the estimated wavelength:

$$\lambda_{KH} = U_c/f_{c,0}, \quad (5)$$

where $f_{c,0}$ is the first cavity resonant mode and U_c is the vortex convection velocity. The value of the convection velocity is assumed to be $U_c = U_\infty/2$, which is commonly found in literature (*e.g.* (Ma *et al.*, 2009; Kook & Mongeau, 2002)). *A posteriori* measurements of λ_{KH} were carried out during the post-processing phase using a simple tracking vortex algorithm which identifies, using a pressure threshold connected isosurfaces surrounding an instantaneous pressure local minimum. The vortex location is considered to be the center of mass of this region. The measured and the estimated large-scale KH rollers length scales are summarized in the Table 1. While the measured and the estimated size of the vortices is in good agreement with Equation (5) for the cases A2, A3, A4. In the case A1 the estimation disagree by a factor two with our measurements. We may argue that the development of the rollers is constrained by a short liner streamwise length $L_{liner} = n_{cavities}d_x$. In fact, the ratio of the estimated wavelength to the liner length $\lambda_{KH,A1}/L_{liner} = 0.65$, while for other cases $\lambda_{KH}/L_{liner} \leq 0.32$ which might indicate the limiting ratio for which the finite liner length has little influence on the KH roller development.

5 Grid Sensitivity Study

In order to study the solution sensitivity to the grid, the baseline grid was refined in the streamwise direction over the liner, thus doubling the number of cells per cavity from $n_x = 20$ to $n_x = 40$. Figure 5 shows the time-averaged wall-normal velocity fluctuation profile extracted in the $n = 50$ cavity at $y = -10d$. At this altitude, the fluid inside the cavity is not entrained by the external flow, as seen from the Figure 2. Since the motion is primarily driven by an acoustic standing wave, the fluctuation velocity profile is symmetrical, with its maximum located near the wall. Both

Case	Measured $\frac{\lambda_{KH}}{d_x}$	$\frac{\lambda_{KH}}{d_x} = \frac{U_c}{f_{r,n} d_x}$
A1	27	50
A2	20	25
A3	16	17
A4	13	13

Table 1: Comparison of the *a-posteriori* measured large-scale Kelvin-Helmholtz rollers wavelength versus the *a-priori* estimation $\lambda_{KH} = U_c/f_{r,0}$, where U_c is assumed to account for $0.5U_\infty$

profiles match very well, which indicates sufficient resolution of both acoustic boundary layer and the standing wave.

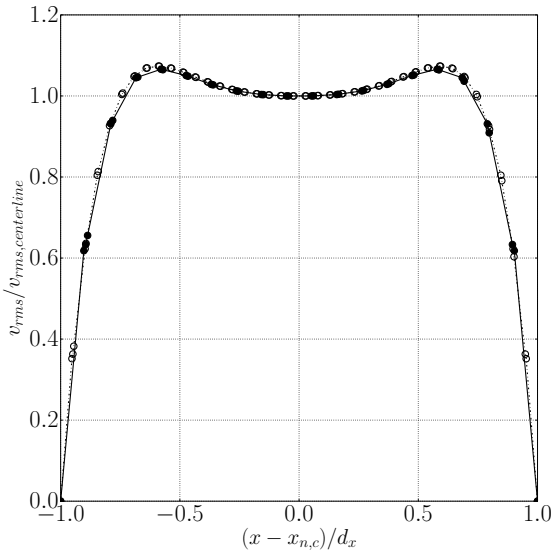

Figure 5: Study of the solution sensitivity to the grid. The time-average root-mean square vertical velocity profile inside the cavity $n = 50$ extracted at $y/d = -10$ in case A1 for two grids. (filled circles) $n_x = 20$ cells/cavity; (hollow circles) $n_x = 40$ cells/cavity.

The time-averaged root-mean square velocity fluctuation and the Reynolds stresses $\overline{u'v'}$ profile were extracted in the cavities $n_i = 1, 15, 25, 75$, thus representing the spatial flow statistics evolution from the upstream edge of the lined zone until the downstream edge. As shows the figure 6.b , both fluctuation profiles are in very good agreement, This indicates that the refinement of the grid has a negligible influence on both the recirculation region inside the cavities, and on the flow over the cavities influenced by the Kelvin-Helmholtz instability.

6 Perspectives and future work

We have investigated the instability mechanism generation in the case of flow-excited two-dimensional idealized liner composed of an array of deep cavities separated by zero-thickness inter-cavity walls (liner porosity $\sigma = 100\%$).

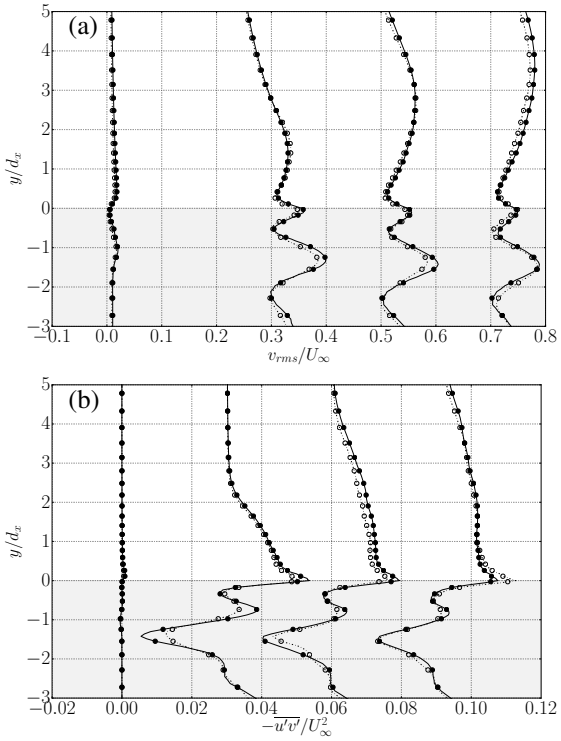

Figure 6: (a) Wall-normal time-averaged velocity fluctuation profile and (b) Time-averaged Reynolds stresses $\overline{u'v'}$ extracted at the cavities $n_i = 1, 15, 25, 75$ centerline, in the A1 case for two grids (filled circles) $n_x = 20$ cells/cavity; (hollow circles) $n_x = 40$ cells/cavity. The gray part of the plot indicates the region lying inside the cavities

In the present work, the incoming flow is laminar at Mach number $M = 0.3$. In contrast to the previously conducted theoretical and numerical studies dealing with a similar configuration where the liner was modeled by Impedance Boundary Condition, the cavities are included in the computational domain thus preserving the discrete cavity-by-cavity nature of the problem. The flow in the entire domain is resolved using fully compressible unsteady Navier-Stokes equations.

The flow response to the variation of the discrete cavity resonance range of frequencies given by was studied by varying directly the cavity depth, while keeping other simulation parameters constant. The progressive reduction of cavity depth in the cases A2-A3-A4 (thus to the shift of all cavity resonant modes toward higher frequencies) resulted in strong coupling of the high ($m > 1$) cavity resonance modes to the shear layer flapping frequency in upstream liner's cavities. This coupling leads to a high instability amplification ratios leading to the shear layer roll up over a short distance. The rollers convected downstream will eventually merge, which decreases the excitation frequency associated to the roller and increases its wavelength. The merging process switches the cavity excitation mode. In the A1 case, the $m = 1$ mode is convectively amplified until the linear instability growth mechanisms saturation which corresponds again to the shear layer roll-up. Consequently, the flow in the downstream part of the liner is dominated by the large-scale vortex structures scaling as $\lambda_{KH} = U_c/f_{r,m}$,

where $U_c \approx 0.5U_\infty$. Overall, the results suggest that the array of subsequent deep cavities has a potential for passive flow control, *i.e.* such devices would allow to introduce the perturbations at a desired frequency controlled by the cavity depth, while the energy is extracted from the mean flow.

Further effort will be also invested to extend existing feedback loop models describing self-sustained cavity oscillations onto a multiple-cavities case.

REFERENCES

Bodart, Julien, Shelekhov, Grigory, Scalo, Carlo & Joly, Laurent 2017 Separation delay via hydro-acoustic control of a naca4412 airfoil in pre-stalled conditions. In *55th AIAA Aerospace Sciences Meeting*, p. 1452.

Brandes, M. & Ronneberger, D. 1995 Sound amplification in flow ducts lined with a periodic sequence of resonators. *Proceedings of the First AIAA/CEAS* .

Burak, Markus O, Billson, Mattias, Eriksson, Lars-Erik & Baralon, Stephane 2009 Validation of a time-and frequency-domain grazing flow acoustic liner model. *AIAA journal* **47** (8), 1841–1848.

Elder, SA, Farabee, TM & DeMetz, FC 1982 Mechanisms of flow-excited cavity tones at low mach number. *The Journal of the Acoustical Society of America* **72** (2), 532–549.

Hirschberg, Avraham & Rienstra, Sjoerd W 2004 An introduction to aeroacoustics. *Eindhoven university of technology* .

Ho, Chih-Ming & Huang, Lein-Saing 1982 Subharmonics and vortex merging in mixing layers. *Journal of Fluid Mechanics* **119**, 443–473.

Jüschke, Matthias 2006 Akustische beeinflussung einer instabilität in kanälen mit überströmten resonatoren. PhD thesis, Ph. D. thesis.

Kook, Hyungseok & Mongeau, Luc 2002 Analysis of the periodic pressure fluctuations induced by flow over a cavity. *Journal of Sound and Vibration* **251** (5), 823–846.

Ma, Ruolong, Slaboch, Paul E & Morris, Scott C 2009 Fluid mechanics of the flow-excited helmholtz resonator. *Journal of Fluid Mechanics* **623**, 1–26.

Marx, David & Aurégan, Yves 2010 Comparison of experiments with stability analysis predictions in a lined flow duct. In *In: 16th AIAA/CEAS Aeroacoustics Conference; AIAA-2010-3946.*, pp. 1–17.

Marx, David, Aurégan, Yves, Bailliet, Hélène & Valière, Jean-Christophe 2010 Piv and ldv evidence of hydrodynamic instability over a liner in a duct with flow. *Journal of Sound and Vibration* **329** (18), 3798–3812.

Meyer, Erwin, Mechel, Fridolin & Kurtze, Günther 1958 Experiments on the influence of flow on sound attenuation in absorbing ducts. *The Journal of the Acoustical Society of America* **30** (3), 165–174.

Michalke, Alfons 1965 On spatially growing disturbances in an inviscid shear layer. *Journal of Fluid Mechanics* **23** (03), 521–544.

Moreno, Iván B., Campo, Laura, Larsson, Johan, Bodart, Julien, Helmer, David & Eaton, John K. 2014 Confinement effects in shock wave/turbulent boundary layer interactions through wall-modelled large-eddy simulations. *Journal of Fluid Mechanics* **758**, 5–62.

Rienstra, S. W. & Darau, M. 2011 Boundary-layer thickness effects of the hydrodynamic instabilty along an impedance wall. *J. Fluid Mech.* **671**, 559 – 573.

Scalo, C., Bodart, J. & Lele, S. K. 2015 Compressible turbulent channel flow with impedance boundary conditions. *Phys. Fluids* **27** (035107).

Scalo, Carlo & Rahbari, Iman 2015 Hydro-acoustic instabilities in compressible turbulent channel flow with porous walls. *The Journal of the Acoustical Society of America* **60** (6), 1397–1405.

Tam, Christopher KW & Auriault, Laurent 1996 Time-domain impedance boundary conditions for computational aeroacoustics. *AIAA journal* **34** (5), 917–923.

Xin, Bo, Sun, Dakun, Jing, Xiaodong & Sun, Xiaofeng 2016 Numerical study of acoustic instability in a partly lined flow duct using the full linearized navier–stokes equations. *Journal of Sound and Vibration* **373**, 132–146.

Zhang, Qi & Bodony, Daniel J. 2016 Numerical investigation of a honeycomb liner grazed by laminar and turbulent boundary layers. *Journal of Fluid Mechanics* **792**, 936–980.